

Comparative detection and fault location in underground cables using Fourier and modal transforms

Vahdat Nazerian¹, Mohammad Esmail Zakerifar², Mahmoud Zadehbagheri³,
Mohammad Javad Kiani³, Tole Sutikno^{4,5}

¹Department of Electrical Engineering, University of Mazandaran, Babolsar, Iran

²Department of Electrical Engineering, Islamic Azad University, Sari Branch, Sari, Iran

³Department of Electrical Engineering, Islamic Azad University, Yasooj Branch, Yasooj, Iran

⁴Department of Electrical Engineering, Universitas Ahmad Dahlan, Yogyakarta, Indonesia

⁵Embedded System and Power Electronics Research Group, Yogyakarta, Indonesia

Article Info

Article history:

Received Jul 2, 2022

Revised Aug 9, 2022

Accepted Aug 20, 2022

Keywords:

Fault location
Fourier transform
Power cable
Short circuit fault
Underground cables

ABSTRACT

In this research, we create a single-phase to ground synthetic fault by the simulation of a three-phase cable system and identify the location using mathematical techniques of Fourier and modal transforms. Current and voltage signals are measured and analyzed for fault location by the reflection of the waves between the measured point and the fault location. By simulating the network and line modeling using alternative transient programs (ATP) and MATLAB software, two single-phase to ground faults are generated at different points of the line at times of 0.3 and 0.305 s. First, the fault waveforms are displayed in the ATP software, and then this waveform is transmitted to MATLAB and presented along with its phasor view over time. In addition to the waveforms, the detection and fault location indicators are presented in different states of fault. Fault resistances of 1, 100, and 1,000 ohms are considered for fault creation and modeling with low arch strength. The results show that the proposed method has an average fault of less than 0.25% to determine the fault location, which is perfectly correct. It is varied due to changing the conditions of time, resistance, location, and type of error but does not exceed the above value.

This is an open access article under the [CC BY-SA](https://creativecommons.org/licenses/by-sa/4.0/) license.



Corresponding Author:

Vahdat Nazerian

Department of Electrical and Computer Engineering, University of Mazandaran

Pasdaran Street, Babolsar, Iran

v.nazerian@umz.ac.ir

1. INTRODUCTION

A fault is a physical condition that results in a device, a component, or an element's failure to perform a required routine. A short or definitive circuit of wire includes this definition. The fault almost always involves a short circuit between the phase conductors or between the phase and the ground [1]. The fault may be an open connection or may have some impedance at the fault connection. The terms "fault", often synonymous with the term "short circuit", are defined in the ANSI/IEEE Std.100-1992 standard [2]–[5]. In fact, methods for determining the fault location for cables are categorized as online and offline. In the off-line method, a special tool is used to test the cable for failure. In the online method, the voltage and current are sampled and their processing is used to determine the fault point. The method of online location for underground cables is different than that used for aerial lines. The two main methods for online location are based on signal analysis and knowledge-based [6]–[9].

In the present study, the travelling wave-based method has been used. Travelling waves are generated by changing the energy stored in the capacitor and the inductor in lines or cables after a fault occurs. Both the voltage and current propagate along the circuit at a velocity close to the velocity of light, encountering impedance discontinuities, and then high-frequency waves emanating from the fault are reflected back to the source and transferred to the other side. What is new in this article is the simultaneous examination of two single-phase faults to the ground with time intervals of 0.3 and 0.305 seconds, with the condition that the faults occur at different points. For this, we used three-phase line and network modeling, fault creation by alternative transient program (ATP) and MATLAB simulator software, and the Fourier and modal transforms to figure out where the faults were.

2. METHOD

A useful analysis of faults in underground cables was carried out, and the travelling waves generated by the fault were discussed and in the form of voltage and current equations presented before, and the method of using these waves was also described in the fault location [10]–[12]. The power cable model is described and a complete model of three-phase power cables is provided [13]–[15]. Subsequently, the discrete Fourier transform (DFT) method will be introduced as a powerful method of discrete Fourier transform for the waves of sampling. Followed by it, the Clarke transform and the transfer of the values obtained from the Fourier transform to the modal domain will be described in this paper. Lastly, to finish talking about finding faults and how to find them, indicators are set up based on the parameters that come from the Fourier transform and how they are moved to the modal domain.

Changes in the amount of stored energy in the inductance and the capacitance of the transmission lines caused by the fault cause to create the travelling waves, that these waves are transferred from the place of occurring fault to two sides of the end of transmission line. The frequency of travelling signals generated by the fault can range from several Hz to several tens of kHz. The path of the traveling wave of travelling waves is plotted in Figure 1 in the event of fault in the F point [16]–[20].

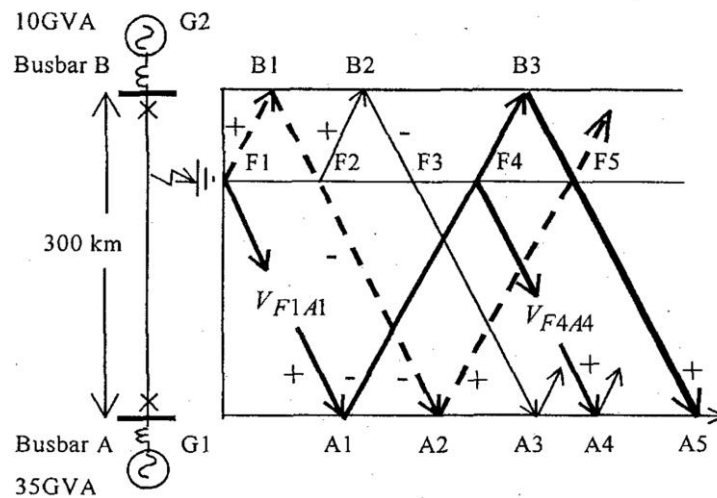


Figure 1. Return of the waves in the case of occurring fault

2.1. Fourier transform

Discrete-time Fourier transform (DTFT) or DFT is one type of Fourier transform. Using this transform, a function (usually defined in the time domain) transmits to another function in the frequency domain, but with the difference that the input function for the DFT transform must be a discrete function. This function or input signal is usually generated by sampling a continuous function such as voltage signals [21], [22]. In general mode, the definition of a discrete Fourier transform is defined as: If $x[n]$, $n \in \mathbb{Z}$ is a discrete function with real or mixed values, then the discrete-time Fourier transform is defined as (1).

$$X(\omega) = \sum_{n=-\infty}^{\infty} x[n]e^{-i\omega n} \tag{1}$$

The equation (1) is considered as the main definition of DFT, which is expressed in terms of discrete signals. If time signal is continuous $x(t)$, in order to obtain the DFT formula, a discrete signal $x'(k\Delta t)$, which contains N samples of the sampled signal $x(t)$, will first be considered that its value is expressed in terms of time as (2):

$$x'(k\Delta T) = x(t)w(t) \sum_{k=-\infty}^{+\infty} \delta(t - k\Delta T) \quad (2)$$

where ΔT is the sampling period and $w(t)$ is the function that contains the N samples of the sampled signal $x(t)$ at a time interval T_0 . In other words, this function can be introduced as a function with the sampling window with length of N. For stable applications, the length of the sampling window is constant, but this window moves forward over time and samples $-\infty$ to ∞ enter and exit from the window, respectively, and thus the sampling process is done during the time domain. But the general form of computing DFT that most authors of articles use are (3).

$$X(r)|_t = (r - 1)\Delta T = \frac{2}{N} \sum_{k=0}^{N-1} x(r + k) e^{-\frac{2\pi}{N}jk}, \quad r \geq 1 \quad (3)$$

In (3), $t = (r - 1)\Delta T$ is the phasor time tag of the sample r. ΔT equal to $1/fs$ is the distance between the two samples of the signal sampled. N is the number of samples in each sampling cycle, which is determined according to the frequency of sampling (fs) and the frequency of the power system (f) ($N = fs/f$). In the above equation $x(r + k)$, the $r + k$ sample is the sampled signal $x(n)$. In real-time applications, there are no later samples in waveform that can be used to calculate the phasor, but the DFT algorithm uses from previous examples to a previous cycle, so there will be a second $N\Delta T$ delay, unless the sampling window changes comparatively with sample variations. In order to adapt to the actual conditions, the phases obtained with the labels can be considered as much as $N\Delta T$ seconds delay or for the real time application, the equation (4) can be used.

$$X(r)|_t = (r - 1)\Delta T = \frac{2}{N} \sum_{k=0}^{N-1} x[(r - 1 + k - N)\Delta T] e^{-\frac{2\pi}{N}jk}, \quad r \geq 1 \quad (4)$$

In this paper, the (4) is used recursively in calculating the phasor of waveform of current. An AC wave can be represented by (5).

$$x(t) = X_m \cdot \cos\left(\phi + \int_{-\infty}^t \omega(\tau) \cdot d\tau\right) \quad (5)$$

For a sinusoidal waveform as defined totally, the term phasor is defined, which is expressed as a vector in the form of a complex number, this complex number includes the size and amplitude of the sinusoidal waveform and its initial angle which will be written as (6).

$$\bar{X} = X_m \angle \phi \quad (6)$$

By applying the DFT defined on the sinusoidal signal, its phasor also obtained that the amount of the Fourier amplitude for the sinusoidal waveform is equal to the amplitude of the sinusoidal signal, but the angular value obtained for the Fourier complex number examples will not be equal to the initial phase angle ϕ and will change for different times. For the first sample of the phasor, the angular amount of the phasor is equal to the initial phase ϕ , but at other times, this value will be changed, such that for the time variations, the periodic variation is between -180° and 180° . In order to eliminate the DFT rotational effect, we use the recursive DFT (RDFT) in the phasor angle of the waveform. In such a way that the difference of the input samples multiplies into the sampling window and samples exiting from the sampling window multiply the amount of fuzzy rotation, /thus, the phase rotation is zeroed over time, and the angle of phasor will be equal to the initial angle. In this way, the RDFF Fourier transform is expressed as (7), ($x(r)$ sample of r^{th}).

$$X(r) = X(r - 1) + \frac{2}{N} [x(r + N - 1) - x(r - 1)] e^{-j\frac{2\pi}{N}(r-1)} \quad r \geq 2 \quad (7)$$

The real time equivalent of the (7) will be as (8).

$$X(r) = X(r - 1) + \frac{2}{N} [x(r) - x(r - N)] e^{-j\frac{2\pi}{N}(r)} \quad r \geq 2 \quad (8)$$

or:

$$(r)|t = (r - 1)\Delta T = X(r - 1)|t = (r - 2)\Delta T + \frac{2}{N}[x((r - 1)\Delta T) - x((r - 1 - N)\Delta T)]e^{-j\frac{2\pi}{N}r} \quad r \geq 2 \quad (9)$$

By obtaining the phasor specifications of the voltage and current waveforms in the network, accurate information can be obtained regarding the characteristics of the voltage and current waves, and many of the events occurring on the network can be detected and identified through changes detected in the amplitude and the angles of measured voltages and currents. Calculating waveform phasor by the discrete Fourier transform as a powerful tool, which can be used in many applications, such as network mode estimation, and the estimation of aerial and cable transmission parameters (as the voltage and current components measured in the previous section is described as phasor), calculations of short circuit faults, sustainability issues, and many cases [21], [22].

2.2. Clarke's transform

The three-phase lines have considerable electromagnetic coupling. In order to eliminate the coupling effect between phases and using the travelling wave's method, the phase domain signals are converted into modal components by a modal transform. One of the well-known transforms used for this purpose in this research is the Clarke transform, which is defined as (10).

$$\begin{bmatrix} M_0 \\ M_\alpha \\ M_\beta \end{bmatrix} = \frac{1}{3} \begin{bmatrix} 1 & 1 & 1 \\ 2 & -1 & -1 \\ 0 & \sqrt{3} & -\sqrt{3} \end{bmatrix} \begin{bmatrix} a \\ b \\ c \end{bmatrix} \quad (10)$$

In which a, b, and c, respectively, indicate the voltage or current of phase A, B, and C respectively. The components, M_0 , M_α , M_β , express modal modes. Since the matrix coefficients are real numbers, modal components obtained from phase signals are completely independent of each other. Independence of these quantities makes the calculations easy for any mode and does not place under the influences of other modes. Using this transform, you can calculate the fault in any mode and analyze the results based on it. This transform can also be applied to the three-phase time waves, and to their phasors, in any case, this transform will cause the independence of three-phase inputs. The result is that Clark's transform only performs the transition from the phase domain to the modal, and does not in itself do any particular work, but for the application, other equations should be used to achieve the objectives of the problem. For example, for short circuit calculations, in this paper, and to identify faulty phases and fault location, it should be defined indicators based on voltage and current equations in the modal field and used them for this goal [21], [23], [24]. The general diagram of the comparative detection/location technique based on the Fourier transform based on the equations described in this section is shown in Figure 2.

Voltage and current measurement units are installed at both ends of the line. The three-phase voltages and currents measured at both ends of the line are converted by Fourier transform to the phasor components, the phasors are transmitted in the fuzzy domain by Clark's transform into the modal domain, and on the basis of which the transmission line parameters are estimated approximately. Then, using the detection and fault location indicators that are related to the line characteristics, the occurrence and type of fault and its location will be estimated [25]–[27].

In this section, using the current and voltage samples coincided at the two ends of the transmission line, an index is provided for estimating the fault location. Consider an optional three-phase transmission line shown in Figure 3 that includes the phases a, b, c and the ground system. The system shown in Figure 3 is divided into two parts. The section of the transmission line is drawn in the form of a three-wire to emphasize the transport structure of the line; other parts of the resource for simplicity are represented as a single-line diagram.

In a line, transmission of voltages and currents at a distance of x (km) from the receiving end are interconnected by the differential (11) [28]–[30].

$$\frac{\partial v}{\partial x} = Ri + L \frac{\partial i}{\partial t}, \quad \frac{\partial i}{\partial x} = Gv + C \frac{\partial v}{\partial t} \quad (11)$$

Both v and i are the momentary vectors of 1×3 , and R , L , G , and C are similar to the previous one, all are the matrices of parameters of transmission line. Under the condition of the stable sinus state, the previous equations change as (12).

$$\frac{\partial V}{\partial x} = ZI, \quad \frac{\partial I}{\partial x} = YV \tag{12}$$

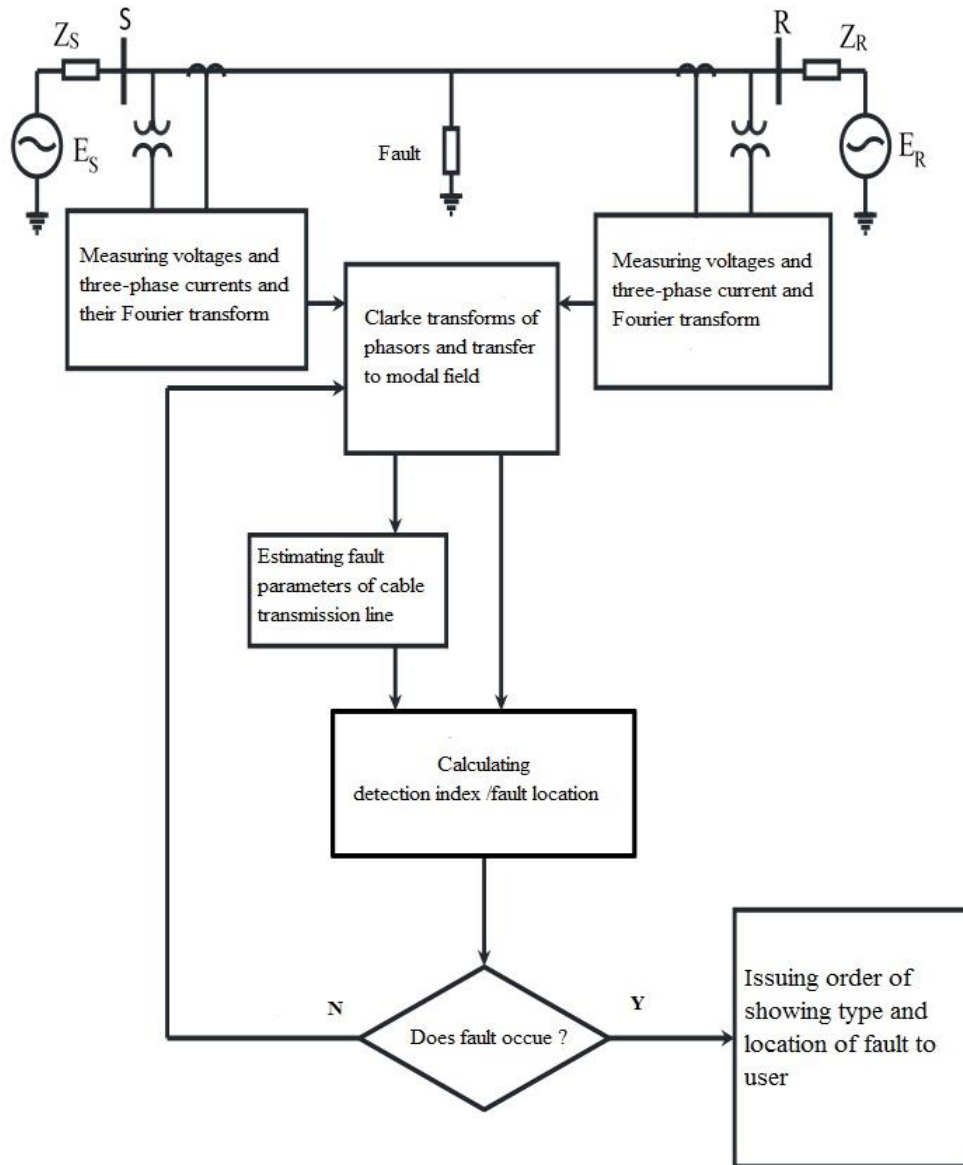


Figure 2. Comparative detection/location system of extra high voltage/ultra-high voltage (EHV/UHV) transmission lines based on Fourier and modal transforms

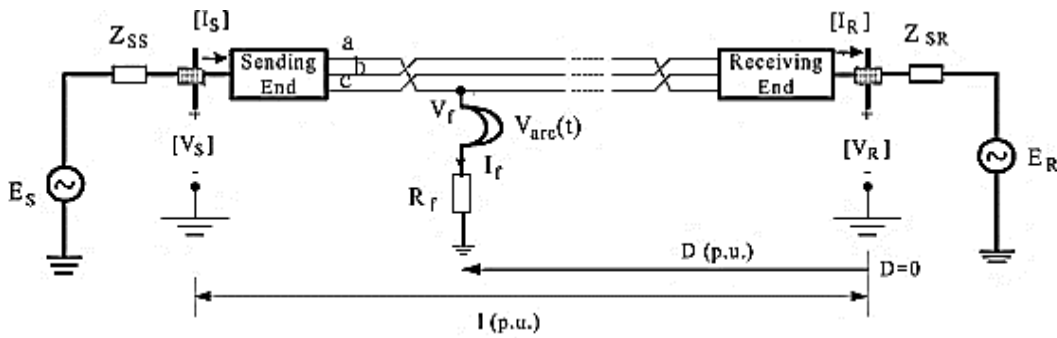


Figure 3. The structure of the three-phase transposed transmission line

Clarke matrix is used to convert distinct fuzzy quantities.

$$\begin{bmatrix} V_a \\ V_b \\ V_c \end{bmatrix} = T \begin{bmatrix} V_o \\ V_\alpha \\ V_\beta \end{bmatrix}, \quad \begin{bmatrix} I_o \\ I_\alpha \\ I_\beta \end{bmatrix} = T \begin{bmatrix} I_a \\ I_b \\ I_c \end{bmatrix} \quad (13)$$

This time, we write this matrix as follows based on the reference article, which does not differ from the matrix T in the previous section.

$$T = \frac{1}{\sqrt{3}} \begin{bmatrix} 1 & 2 & 0 \\ 1 & -1/\sqrt{2} & \sqrt{3}/\sqrt{2} \\ 1 & -1/\sqrt{2} & -\sqrt{3}/\sqrt{2} \end{bmatrix} \quad (14)$$

0 and α and β presents Clarke's components of the voltages and currents, and T is the Clarke's transfer matrix. By solving the above equations, the equation (15) is presented as a phasor response.

$$\begin{aligned} V_m &= \exp(\Gamma_x)A + \exp(-\Gamma_x)B \\ I_m &= \exp(\Gamma_x)Z_C^{-1}A - \exp(-\Gamma_x)Z_C^{-1}B \end{aligned} \quad (15)$$

V_m and I_m , both are phasor vectors of the modal of signals with dimensions 1×3 , and the subscript 0 and α and β are referred for them. Γ and Z_C are constant matrices of propagation of modal and linear wave impedance of line modal in the following form.

$$\begin{aligned} \Gamma &= \sqrt{T^{-1}ZYT} \\ Z_C &= \sqrt{T^{-1}ZY^{-1}T} \end{aligned} \quad (16)$$

Since assumed that the transport line is transposed, the displacement property of the multiplication of matrix was used in the above procedure [31]–[34]. We have the equivalent of the (16) for the single-phase line of the Z_C and γ values $Z_C = \sqrt{(R + j\omega L)/(G + j\omega C)}$ $\gamma = \sqrt{(R + j\omega L)(G + j\omega C)}$. Using the data of measuring phasor (V_S , I_S) and (V_R , I_R), the impedance and propagation constant of the transmission line can be calculated from the two ends of the line inversely. The line parameters are expressed as (17), respectively.

$$\begin{aligned} Z_{Cm} &= \sqrt{\frac{\bar{V}_{Sm}^2 - \bar{V}_{Rm}^2}{\bar{I}_{Sm}^2 - \bar{I}_{Rm}^2}} \quad m = 0, \alpha, \beta \\ \gamma_m &= \cosh^{-1}(K_m)/L \quad m = 0, \alpha, \beta \\ K_m &= \frac{\bar{V}_{Sm}\bar{I}_{Sm} + \bar{V}_{Rm}\bar{I}_{Rm}}{\bar{V}_{Sm}\bar{I}_{Rm} + \bar{V}_{Rm}\bar{I}_{Sm}} \end{aligned} \quad (17)$$

The total values listed above are the modal components of the measured signals derived from the Clarke transform, that subscript m referring to, α and β . In order to avoid the effects of zero modes and the uncertainty of zero mode parameters, zero mode calculations are not recommended [23]. Constants A and B are determined by boundary conditions at the end of the transmitter and receiver. Suppose the fault is occurred in the middle of the line at point F that $x=DL$ km from the end of the receiver R in the transmission line SR of Figure 3. L is the total length of the transmission line; D is the per unit distance from the receiving end to the fault and is also used as an index of fault location/detection. In the case of fault at point F , the transmission line is divided into two sections. One is the SF section and the other is FR . These two sections of the line can still be considered as a complete transmission line. This means that the voltages at each point on the two sections of the line can be expressed in terms of the voltage and current measured at the two ends of the S and R . In addition, at the fault point F the voltages in the expressions of two datasets (V_S , I_S) and (V_R , I_R) is equal. If we placed two measuring datasets (V_S , I_S) and (V_R , I_R) on a reference position $x=0$ and give the boundary conditions at the two ends, the voltage in the fault position $x=DL$ km can be expressed:

$$V_F = \frac{(V_R + Z_C I_R)}{2} \exp(\Gamma DL) + \frac{(V_R - Z_C I_R)}{2} \exp(-\Gamma DL) \quad (18)$$

$$V_F = \frac{(V_S + Z_C I_S)}{2} \exp(\Gamma DL - \Gamma L) + \frac{(V_S - Z_C I_S)}{2} \exp(\Gamma L - \Gamma DL) \quad (19)$$

By equating the voltage at the fault point, the fault location of the D per unit is obtained by (20).

$$D_i = \frac{\ln[(A_i - C_i)/(E_i - B_i)]}{2\Gamma_i L} \quad i = \circ, \alpha, \beta \quad (20)$$

A_i , B_i , C_i and E_i are the elements of vectors A , B , C and E with dimensions 1×3 and $i=1, 2, 3$ are used to represent the modal components \circ , α and β of signals. Γ_i shows the diametric elements of the propagation constant matrix of the 3d-3d modal. We write the (20) in the vector form of (21).

$$D = \frac{\ln[(A-C)/(E-B)]}{2\Gamma L} \quad (21)$$

The values of these signals used in the (21) are as (22).

$$\begin{aligned} A &= \frac{1}{2}[V_R - Z_C I_R] & B &= \frac{1}{2}[V_R + Z_C I_R] \\ C &= \frac{1}{2}e^{\Gamma L}[V_S - Z_C I_S] & E &= \frac{1}{2}e^{-\Gamma L}[V_S + Z_C I_S] \end{aligned} \quad (22)$$

Finally, in order to test the efficiency of the above method in fault location, the percentage fault of the distance between the actual location and the calculated location is used and is defined as (23).

$$\%error = \frac{\text{actual fault location} - \text{calculated fault location}}{\text{Totally fault section length}} \times 100 \quad (23)$$

The above criterion can be used to compare all methods of locating and determining their accuracy and provided a proper assessment of the method's performance. Since fault location in three-phase lines is intended, considering that these lines have significant electromagnetic coupling, in order to remove the effect of coupling between phases and to use the traveling wave method, we convert the phase domain signals into separate modal components by a modal transform, which is a relatively new work.

3. RESULTS AND DISCUSSION

In the present study, an EMTP/ATP software is used for simulation example and, according to it, the cable network is investigated. This is comprehensive software for transient states studies and provides both models of aerial and cable transmission lines. In this paper, the JMarti model for underground cables is used. The model of adjacent cable networks is modeled on a tune on equivalent on both sides of the S and R, with voltage sources of $230 \angle 10$ and $230 \angle 0$.

3.1. Fault simulation in locations with different resistances at different times

After modeling the network and line, two single-phase A to ground (AG) faults occur at different points of the line at 0.3 and 0.305 s times. First, the fault waveforms will be displayed in the ATP software, and then this waveform will be transmitted to MATLAB software, and will be presented along with its phasor view over time. In addition to the waveforms, the detection and fault location indicators are presented in different states of fault. Fault resistances 1, 100, and 1,000 ohms are considered for creating fault and modeling fault with low arch strength to resistance of high fault. In representing the transient waveforms generated by fault and DFT function and detection and location indicators, the figures related to the faults created in phase A are displayed and due to the similarities of other faults, the presentation of the corresponding figures is avoided and the results in relevant tables are presented.

3.2. Single phase A fault in the middle of cable in 0.3 seconds with a fault resistance 1Ω

In this section, a single-phase AG short-circuit fault with a fault resistance 1 ohm is generated at 0.3 seconds in the middle of the cable. It is assumed that the measuring units are installed on both S and R bus, and the voltage and current signals of both ends are measured at any moment. The measured values of voltage and current from both S and R bus are shown in the following diagrams, respectively. The voltage waveform in S bus is shown in Figure 4. As it can be seen in the figure, the voltage is in its stable state before the fault occurs, by creating short circuit fault at 0.3 s, the voltage drops sharply and, after eliminating the fault at time 0.5 s, becomes normal. Transient waves at the same moments of fault quickly disappear.

The above waveform is shown in Figure 5 after transferring to the MATLAB environment and applying the DFT on it. In this paper, the waveform time steps in the ATP software are equal to 10^{-6} . For phasor measurement, the ATP waveforms are sampled at 10 kHz and from samples of DFT Fourier

transform, a frequency of 50 Hz is taken. The sampling window is considered equal to a full power cycle and the number of samples in this window is $N=200$. Due to the constant number of samples in the DFT sampling window, there is a 20 msec delay (a power cycle) after the sudden change of waveform state, which full cycle DFT will not be able to detect rapidly these changes, although after starting waveform changes, these changes are detected in the phasor area by DFT, but due to the incomplete sampling window, rapid changes in voltage waves and short-circuit current are not detected with sufficient speed and accuracy. To increase the tracing speed of changes of transient waves, the length of the sampling window of sampling can be shortened so that the tracing accuracy of the fast changes in the waveform to be increased due to fault, but during normal conditions and slight variations in the amplitude of the waveform, the number of samples and the length of Fourier transform information window should be reached in a full cycle to prevent non-basic frequency oscillations.

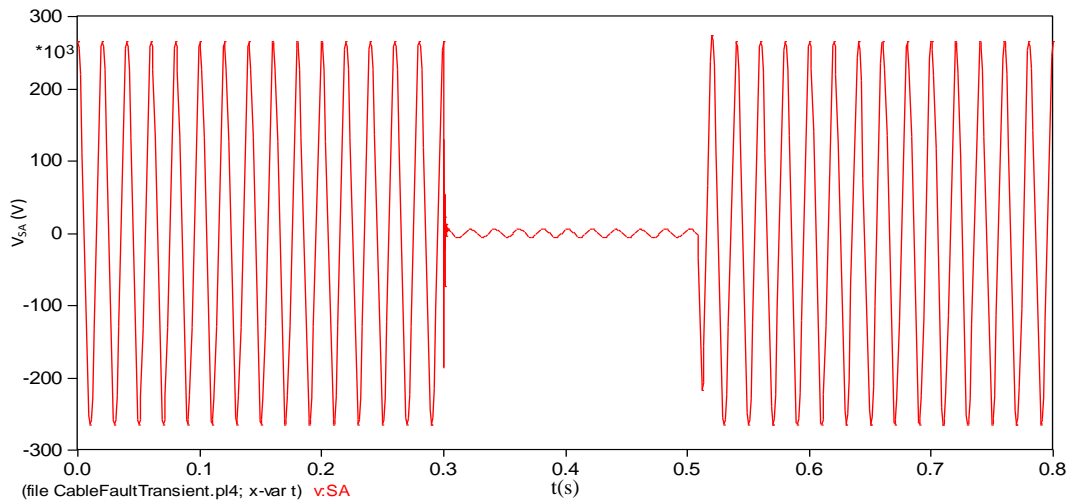


Figure 4. The waveform of the measured voltage of phase A at the bus S

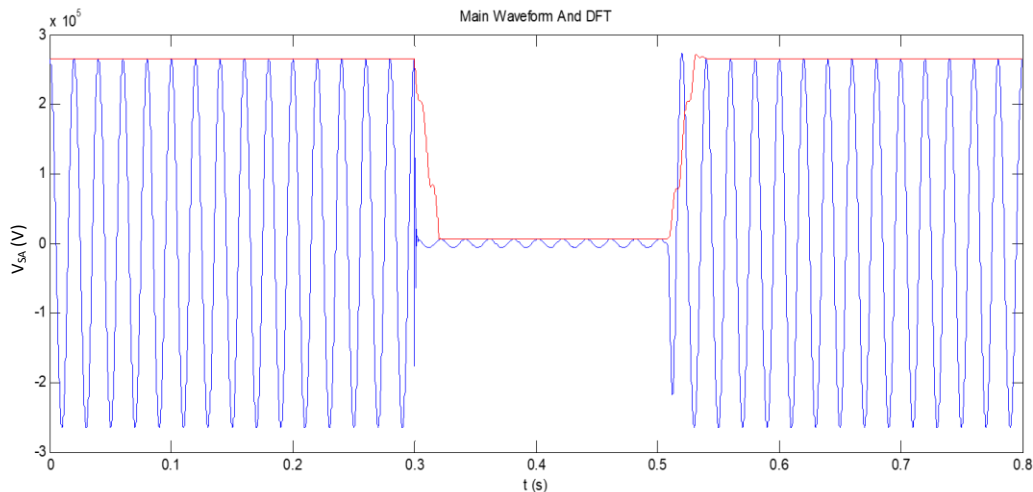


Figure 5. Display the waveform of the A phase voltage in the MATLAB environment and its DFT diagram

To avoid the phase rotation due to moving the DFT information window along the waveform, we use a recursive DFT, so that the phasor angle of the sinusoidal waveform remains constant during steady state. The result of this operation is shown in Figure 6. Figure 6 shows the phasor angle of the measured voltage at the bus S. After the fault occurred at time 0.3 s, in addition to changing the size of the phasor, the angular value also changes, within 0.5 seconds after the fault is resolved, the value of the phasor returns to

the initial value before the fault. As it is seen, due to the recurrence property, fuzzy rotation is not observed at the phasor angle.

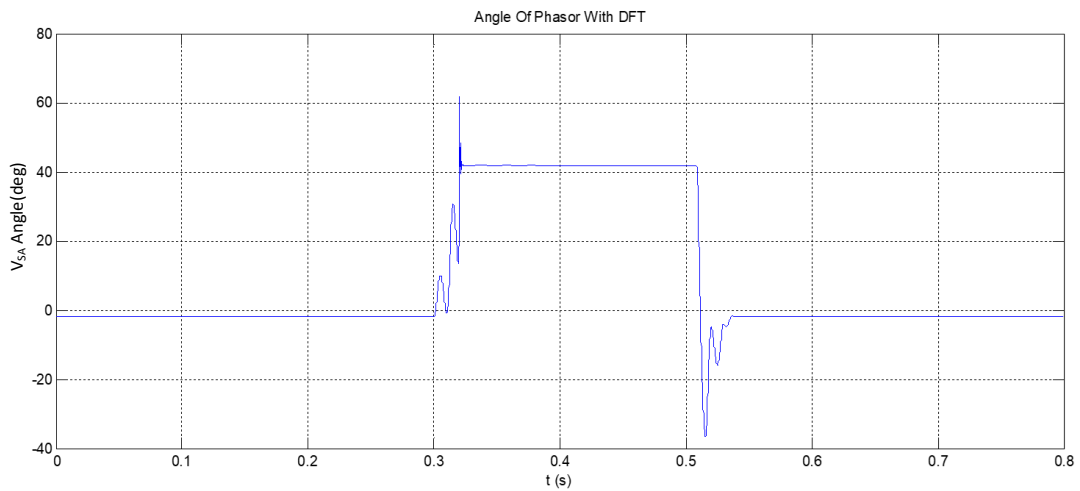


Figure 6. Phasor angle of phase A voltage at bus S

Obviously, during short circuiting, the current through the line will increase suddenly and the voltage of bus connected to it will drop sharply. The simulation result for measured current of phase A at the bus S is shown in Figure 7. Depending on the short-circuit occurrence, in the DC waveform, a decline view with different amplitudes can be created. In Figure 7, the DC component present in a waveform is small. The sampled waveform of the phase A current at the S bus and its phasor size in the MATLAB environment is plotted in Figure 8. Figure 9 shows the phasor angle of the phase A current at the bus S.

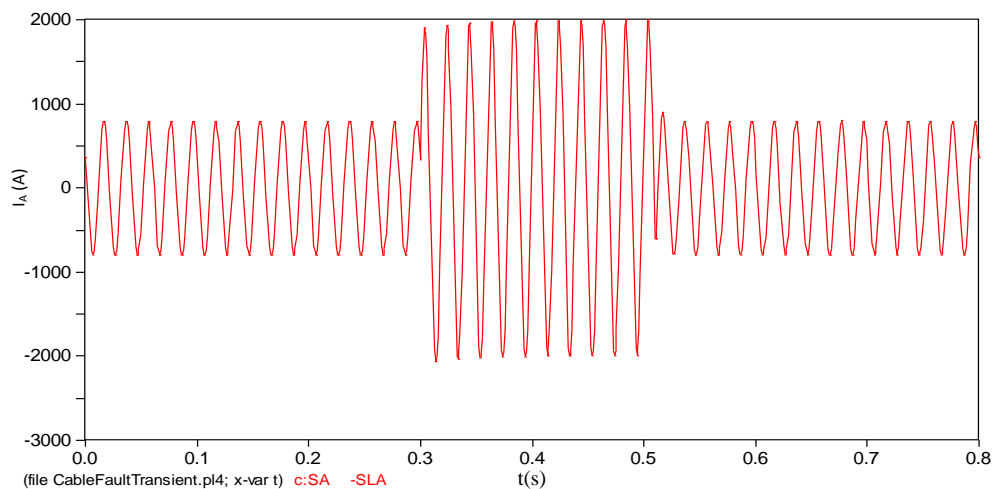


Figure 7. The waveform of the measured current of phase A at the bus S

Due to the fact that single phase fault occurred in phase A, there is strong changes in phase A, but phase B and C are only affected by the induction of phase A variations. However, variations in phase A current have little effect on phase B, and C currents, and this effect is small in the case of the voltage amplitude, which is not visible, but a change is seen at phasor angle of voltage that is not too high. The waveforms of the phases B and C during the phase A fault are stable and uniform. The time waveforms of the phase B and C voltages and phasor amplitude of phase B voltage are shown in Figures 10 and 11, respectively.

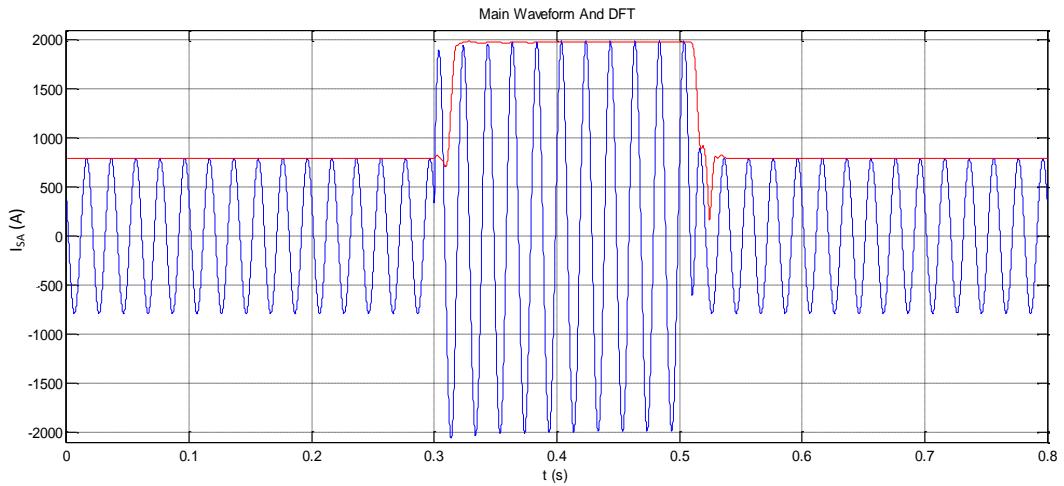


Figure 8. Current waveform sampled at the bus S and its phasor amplitude

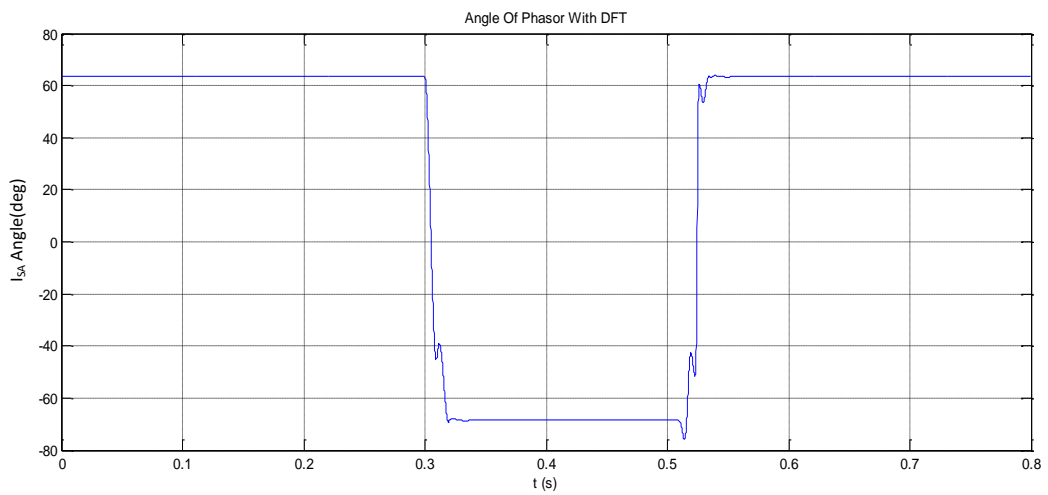


Figure 9. Phasor angle of phase A current at the bus S

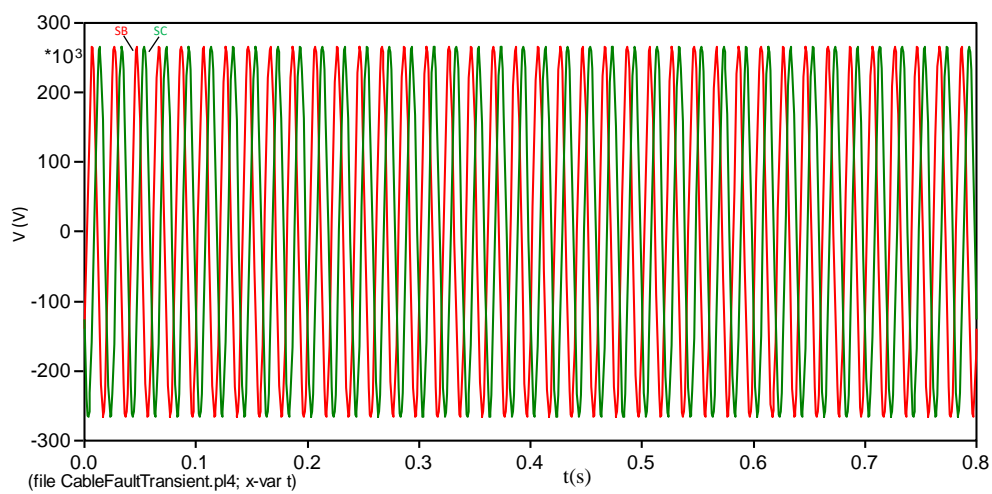


Figure 10. Voltages of phase B and C at bus S

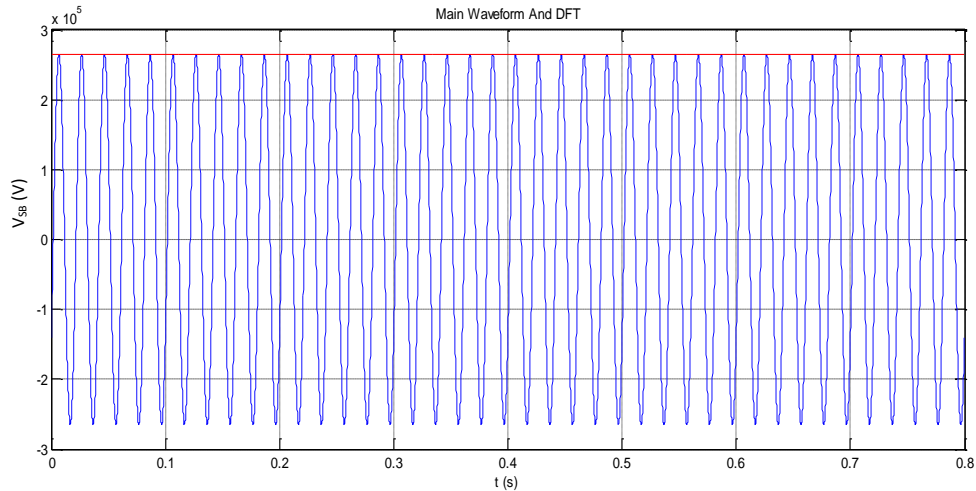


Figure 11. Phasor amplitude of phase B voltage in bus B

Figure 12 shows the variation in the angle of B phase voltage due to fault in phase A, which, according to the figure, it can easily be seen that this change is 0.84 degrees and is negligible. This change shows coupling and the effect of the variations of a phase in the two other phases and states the dependence between them, given the figures of simulation; this dependence can be easily detectable. Figure 13 also shows the waveforms of the phase B and C current. With a little more detailed observation of the time waveform, it is possible to detect the change in the current of phases B and C at moments to start and resolve the fault. The phase B current and its phasor amplitude are shown in Figure 14. Changes in the actual waveform and its phasor amplitude are more evident in this figure.

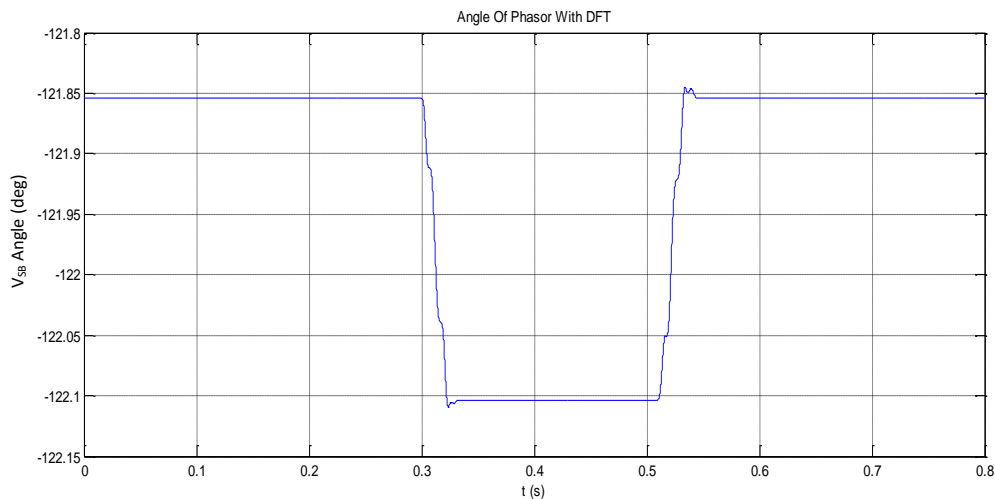


Figure 12. Phasor angle of phase B voltage at bus S

Similarly, the phasor angle of the phase B current is shown in Figure 15. The variations in the phasor angle of the current are about 0.3 degrees and have a small amount. It should be noted that the values of voltage and current in the bus R are also similar to these parameters in the bus S. For fault detection and location, their phasor calculations are required using the Fourier transform in both buses, so to refuse the excessive increase of figures, showing of the actual time-wavelength and phasor on bus R is avoided because the process of variations and appearance of the figures are similar to the parameters of the measurement at bus S.

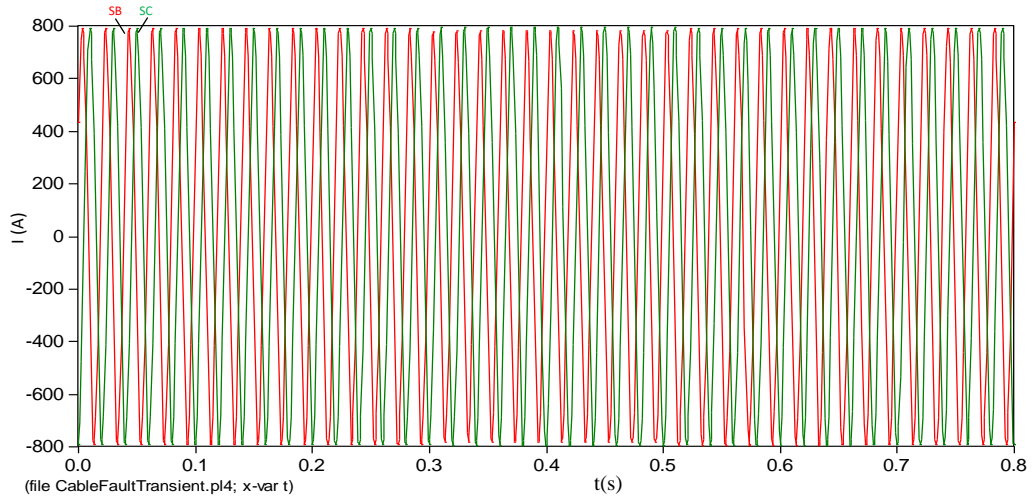


Figure 13. Current of phases B and C at the bus S

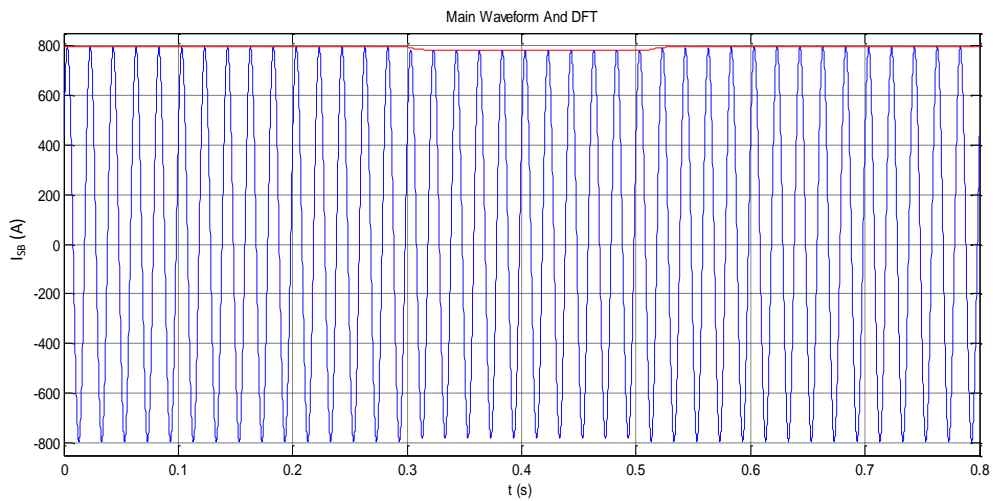


Figure 14. Phase B current and its phasor amplitude

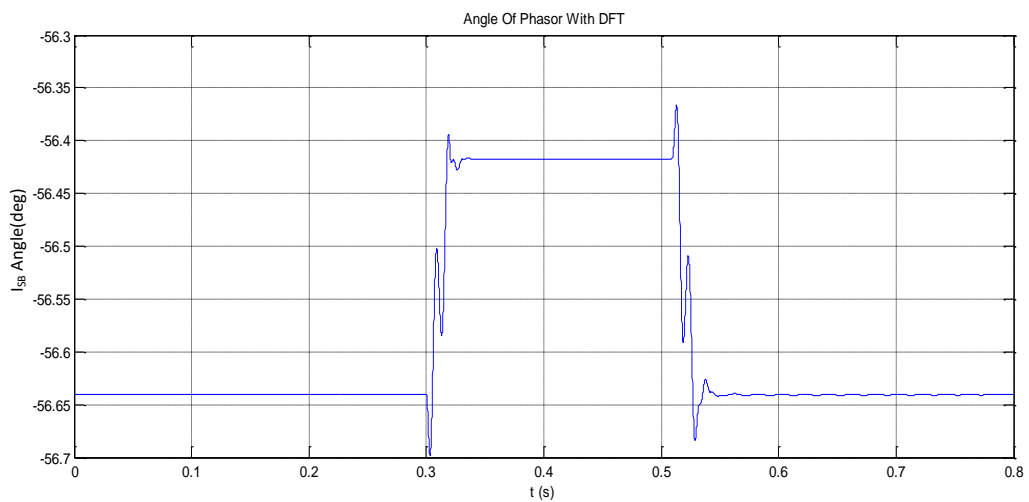


Figure 15. Angle of phasor of phase B current

After obtaining and displaying the waveforms of the size and angle of phasors of voltage and current of phases, calculations related to the transfer of voltages and currents from the fuzzy domain to the modal domain using the Clarke transform, and then the calculations related to the detection indicators of type of fault and its location during the power cable are performed, and thus the type of fault and its location are identified and the corresponding figures are gradually displayed. Although in almost all articles related to the calculations of identification and classification of fault location using impedance methods and the use of indicators of fault location, calculations in the modal domain have been proposed. In this paper, we use the calculations of M and N fault detection indices in the fuzzy domain, along with the calculations of the detection indicators in the modal field. But about the location indicators, we only use the D location index in the modal domain. All calculations for fault detection indices in the fuzzy and modal domains are the same, but the only difference is the use of Clarke's transform.

First, the line parameters for the stable conditions before the fault are estimated using the equations described in the previous section based on the DFT phasors on the voltage and current of the three-phase of the primary and terminal two-bus and then using the values of the estimated parameters of the coefficients of distribution and impedance of the cable characteristic and equations related to the calculation of the indicators, their values are calculated in the fuzzy and modal domains. We use the α mode about location index, because it has the least computational fault in detecting the location of the transmission lines and cables in different types of faults, in other words, in the types of single-phase, two-phase and three-phase faults, this index is more successful than the beta and zero mode indicators. In this study, we use this index to determine the fault location in cable. In terms of performance, the fault detection indicators operate both in the fuzzy domain and in the modal domain, so that, with the occurrence of the fault, the values of both the M and N indices increase from the very low value almost zero to a great value more than 10^3 order, as soon as the fault is resolved, it decreases again to a value of zero, even if it the network becomes unstable. However, the more the fault of the short circuit is occurred with the lower fault resistance, the value of these indicators will be greater, and vice versa, with increasing the fault resistance, their values decrease. Therefore, the condition for increasing these indexes more than a certain value, which in this paper is greater than 500 for the index $N_{a, b, c}$, and for the index $M_{\alpha, \beta, 0}$ to detect single-phase fault of AG greater than 1,000 and for other faults is selected greater than 700, the choice of the type of N indices in the fuzzy domain and the M in the modal domain is based solely on decision making on the interference of both indicators in decision making and has no other basis and it is possible to arbitrarily select each combination of the two N And M indicators in the phase and modal domains that have no effect on the result. The choice of the above numerical values is also based on the characteristics of the network studied and can be chosen differently for different networks; only it should be paid attention to this issue that the selected boundary numbers should be chosen in such a way that for different fault resistances from zero to high values to be given a correct answer. The values in this network have been selected after trying and fault for different fault and values of different fault resistance. Regarding the use of fuzzy indicators to detect the type of fault, it should be noted that although the three-phase parameters are not independent and mutually influential, but the ratio of the effect of changes in a phase on the two other phases is not such that the induced variations to be influential as much as the intensity of phase (fault) and its effect is small, on the other hand, in the fault indicators, because the voltage and current information of both buses is used, and the corresponding parameters differently from each other according to the characteristic impedance are reduced, the indices of detection act like the method used in differential relays and their values in faulted phases is much more than faultless phases. In faultless phases, although there is a disturbance due to the negative effect of the fault phase, but because of having the difference property of the parameters of the two primary and terminal buses, their values will be little, it can be deduced that the detection indices in the fuzzy domain can also be used to identify the type of fault, which is confirmed by repeated simulations and its results.

Figure 16 shows the detection indicator of fault $N_{a, b, c}$. It is seen from the figure that all three fault detection parameters in the moments before the fault are equal to zero, but after fault in the phase A at 0.3 seconds, the N_a value increases from zero value to a large value, if values N_b and N_c are still equal to zero and do not change, and will always be equal to zero. After removing fault, the fault detection value of the phase A (N_a) decreases again to zero. Simultaneously, Figure 17 shows the values of the fault detection index in the three modes α , β and 0, as it can be seen that all three fault indices N_α , N_β and N_0 are zero before the fault and as soon as the fault occurs, simultaneously increase to a large value and after removing fault in phase A, they return to zero. By observing this situation, it can be easily understood the result. Although the modal detection indicators are suitable for detecting the fault state, but the type of fault cannot be correctly identified with these indices, in short circuit fault of single-phase B and C, the same situation occurs (changing all three modal indicators), and so in this study, we use the fuzzy detection index calculations to determine the fault type and the fault phase, which also obtains a correct result.

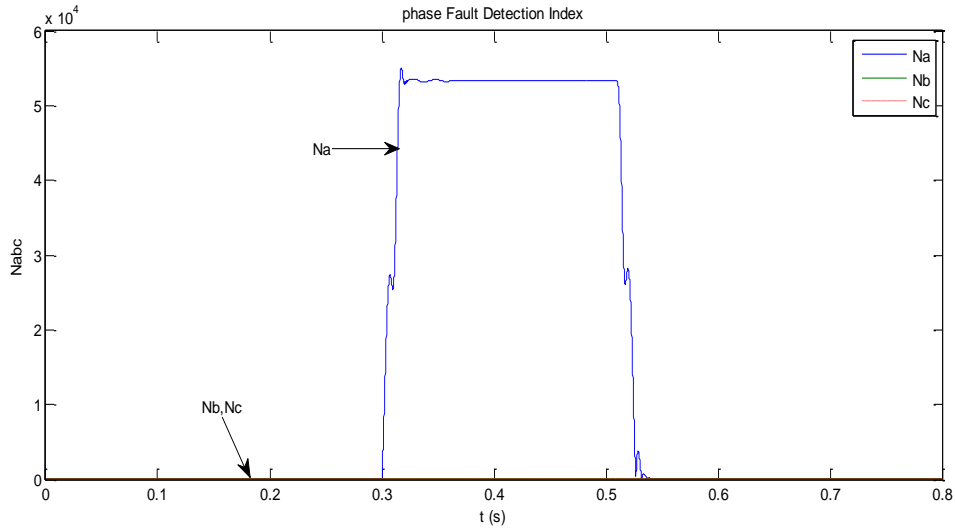
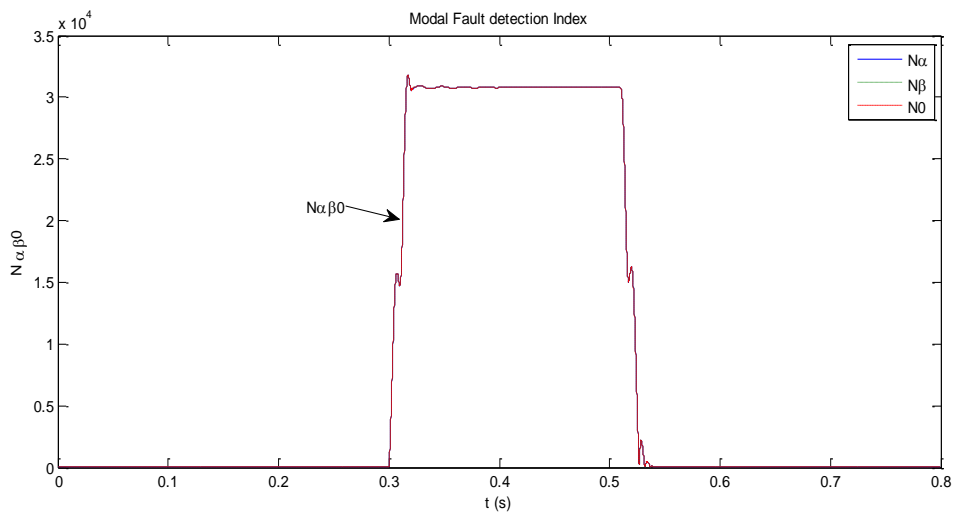


Figure 16. Fuzzy fault detection indicator

Figure 17. Modal fault detection indicator of $N_{\alpha\beta 0}$

In the case of the fault location index, the situation is different, so that due to the small amount of this indicator, both in fault and in other circumstances, from normal to the state of the existence of disturbances other than fault in the system, modal values have sufficient citing and required accuracy to identify the fault location in the modal area, and in the fuzzy field, according to the citing articles are not used. Also, since this index is obtained by dividing the two N and M fault detection indicators, the disturbances and the effects of the fault in the healthy phases also make relatively significant changes. However, according to various papers and repeated experiments, the result is obtained that the use of the D index in α mode has the highest success among other mods, and therefore, in this simulation, this parameter is used to determine the location of fault, and as the next results will show, this parameter correctly shows the fault location.

Figure 17 shows the values of fault location indices in the modal domain for the three modes α , β and zero $D_{\alpha\beta 0}$. It is noticeable that the values of this index in three modes before the fault have different values greater than one. As the error occurs in phase A in 0.3 seconds, all three location indexes of D_{α} , D_{β} and D_0 reaches to 0.5. If the value of this index reaches a number between zero and one, and in addition, the fault detection indices is a large number, then it can be stated that fault occurs between the two buses R and S, and the result of the multiplication of the fault location in the total length of the cable, the distance from

the fault location is obtained from the bus R. With this description, it is clear that in the case of a single-phase fault AG in the middle of the cable, the D_α index presents the middle position of the cable as the fault location, which is a perfectly correct result, and this value is observed in simulated figures.

After the error occurred, the value of these indicators were changed from 0.5 to an undefined amount and over time, different values are obtained, sometimes the value of this index reaches a number between 1 and zero, but since the value of the detection index is zero, it cannot be stated that fault has occurred, while at the time of occurring fault, this number remains in the specified value between zero and a constant after a few moments, but in turbulence conditions or in other conditions such as the oscillation of power, if the index value reaches a number smaller than one, it does not remain constant. The irregular behavior of the index D after the fault in Figure 18 is because, since the M and N values are very small and zero at non-fault conditions, the smallest variations in them, due to their division, can cause large, rapid and irregular changes in D index. Before the fault occurs, the calculation fault is related to the entire sampling process and the DFT application is zero, due to the recursive property of the DFT, the TVE fault of the phasor samples is accumulated over time, after the error occurred because in addition to the main frequency, other frequencies appear in the waveform; these frequencies, which are located within the Fourier transform, are not completely eliminated and cause fault in calculating the base frequency phasor (while non-known frequencies near the main frequency will also appear in the waveform) that these faults will be due to the recursive DFT within it. Although the DFT itself eliminates many of the frequencies due to inherent filtering properties and the error value is low, it shows its effect in calculating the values of the M and N indices in the mode after removing short-circuit fault. Therefore, it can be seen that after removing fault, fluctuations in the D index are updated.

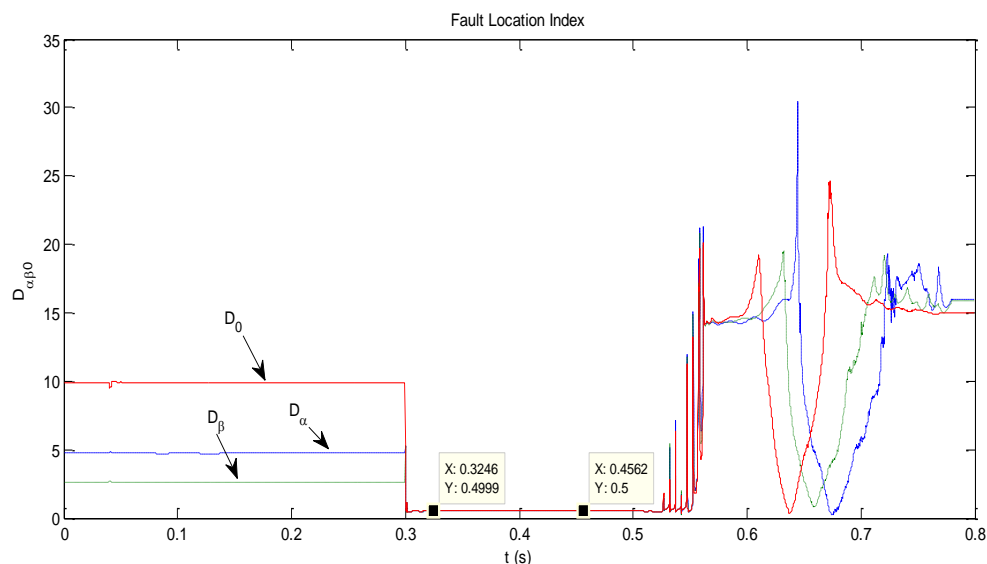


Figure 18. $D_{\alpha,\beta,0}$ fault location indicators

Among the many simulations carried out, in this section, the simulation of single-phase faults of AG for 1, 100, and 1,000 ohms resistances at 0.300 and 0.305 s times at different points of the cable at intervals of 50, 25, 10 and 2.5% of the power cable length from the bus R is shown in the Tables 1 to 4 respectively, and the type and locations of the calculated faults and their time and calculation fault are presented. Calculations of other faults in different places and times can also be done and see the results. In this section, this simulation is satisfied and, of course, the calculations are available in other conditions such as the present modes. First, the calculations of fault in the fault location created in the middle of the cable are shown in Table 1. According to the classification, the generated faults are AG type, respectively, that fault resistances are considered 1, 100, and 1,000 ohms. For each fault resistance, the times 0.3 and 0.305 s are considered in the next row. Afterwards, the performance of the fault detection index and the time of detection are shown in the subsequent rows. In the case of fault detection time, it can be seen that by increasing the fault resistance value according to the constant numerical criteria 500 and 700 for the fault detection index for all faults, the fault detection time also increases, because the changes in the fault detection indicator in mode of high resistance fault is less than low resistance fault.

Table 1. Types of faults in the middle of cable and index of detection and location and its detecting time

Time of finding fault location with percentage fault	Percentage of fault of location	Fault location (km)	Value of fault location index	Time of detecting type of fault (s)	Time of occurring fault	Fault resistance	Type of fault	Distance of fault from source
0.3263	0.0062%	20.0025	0.49993	0.3006	0.3s	1	AG	20 km 50%
0.4298	0.0805%	20.0322	0.49919	0.307	0.305 s			
0.3327	0.0117%	20.0047	0.49988	0.3017	0.3s	100		
0.3382	0.0022%	20.0009	0.49997	0.3083	0.305 s			
0.3415	0.0007%	20.003	0.49999	0.3115	0.3 s	1000		
0.3425	0.006%	20.0024	0.49994	0.3187	0.305 s			

Table 2. Fault in 25% cable relative to bus R and index of detection and location and its detecting time

Time of finding fault location with percentage fault	Percentage of fault of location	Fault location (km)	Value of fault location index	Time of detecting type of fault (s)	Time of occurring fault	Fault resistance	Type of fault	Distance of fault from source
0.3388	0.0782%	30.0313	0.2492	0.3009	0.3 s	1	AG	30 km 75%
0.4689	-0.0767%	29.9693	0.2508	0.3069	0.305 s			
0.3326	0.0087%	30.0035	0.2499	0.3016	0.3 s	100		
0.3391	-0.006%	29.9973	0.2501	0.3082	0.305 s			
0.3407	0.0039%	30.0012	0.2500	0.3114	0.3 s	1000		
0.3429	0.019%	30.0076	0.2498	0.3193	0.305 s			

According to the table, except for a single-phase fault 1,000 ohms in phase A, in the rest of the cases, the definite detection time of fault has been less than 5 ms after occurring fault. For example, for single-phase fault AG, the fault resistance of 1 ohm after the fault in 0.3 s, only 0.6 ms, after which the single-phase fault AG was detected, and in the fault generated at 0.305 s, after 2 ms, type of fault is detected. The maximum detection time also belongs to the AG fault at 0.305 s with a resistance of 1 ohm, which is 0.4289. It should be considered that the time of detection and removing fault should be less than the critical time to resolve the fault in the study network. The more the time is less, the necessary measures are taken place to prevent network instability and repairs faster and the network undergoes less stress. In almost any article, the time of detection of fault location is not referred, and then this time is mentioned in this research. This time is very important in online methods for locating fault. However, in this case, absolute optimization was not carried out and the purpose was to find the fault location with a percentage of less faults. If it is necessary, this time is as small as possible, phasors with an adaptive window length can be used, or considered the criterion as the average of the maximum and minimum values after two consecutive maximum values and two consecutive minimum are within a specified range that in this situation, even before the index D reaches to a stable state and to be stable, it can be accurately expressed the value as the index of the output location of program. It is emphasized again in this paper, as in all previous articles [23], [25], [28], [31], that the accuracy of the location index is preferable to the time required to find it (albeit to an acceptable level).

Table 3. Fault in 10% cable relative to bus R and index of detection and location and its detecting time

Time of finding fault location with percentage fault	Percentage of fault of location	Fault location (km)	Value of fault location index	Time of detecting type of fault (s)	Time of occurring fault	Fault resistance	Type of fault	Distance of fault from source
0.3588	0.1367%	36.0539	0.0987	0.3012	0.3 s	1	AG	36 km 90%
0.4889	-0.0370%	35.9852	0.1004	0.3078	0.305 s			
0.3326	0.0691%	36.0277	0.0993	0.3016	0.3 s	100		
0.3394	0.0495%	36.0198	0.0995	0.3081	0.305 s			
0.3403	0.0627%	36.0251	0.0994	0.3114	0.3 s	1,000		
0.3468	0.0626%	36.0251	0.0994	0.3193	0.305 s			

Table 4. Fault in 2.5% cable relative to bus R and index of detection and location and its detecting time

Time of finding fault location with percentage fault	Percentage of fault of location	Fault location (km)	Value of fault location index	Time of detecting type of fault (s)	Time of occurring fault	Fault resistance	Type of fault	Distance of fault from source
0.3488	-0.0063%	38.9975	0.0251	0.3012	0.3 s	1	AG	39 km 97.5%
0.4888	-0.0026%	38.999	0.02502	0.3082	0.305 s			
0.3326	0.128%	39.0512	0.0237	0.3017	0.3 s	100		
0.3395	0.1055%	39.0422	0.0229	0.3083	0.305 s			
0.3402	0.1205%	39.0482	0.0238	0.3114	0.3 s	1,000		
0.3467	0.1192%	39.0477	0.0228	0.31192	0.305 s			

4. CONCLUSION

In this paper, the problem of fault detection and its location in underground three-phase power cables has been investigated. The use of detection and fault detection indices in the fuzzy field is based on the Fourier transform of voltage and current signals, which provides a correct answer in identifying the type of fault. In addition, the fault detection modal indices prove the fault occurrence, but they cannot be used to accurately detect the type of fault, and fuzzy detection indices should be used. The fault location index in the modal domain in α mode is considered as the basis in determining the fault location. The use of the above indicator in the determination of the fault location is less than 0.25%. This fault is quite appropriate in the references according to the value of the fault, although the location of the fault is varied for changing the conditions of time and resistance and the type of fault and its location, but not exceeding the above value. From the results mentioned in this paper, we will conclude that the use of Fourier transforms and modal transforms with the use of fault detection and location indicators is very effective in determining the type and location of fault, and this subject is repeatedly expressed in various sections of this paper and shown.

REFERENCES

- [1] B. Kasztemy, I. Voloh, C. G. Jones, and G. Baroudi, "Detection of incipient faults in underground medium voltage cables," in *61st Annual Conference for Protective Relay Engineers*, Apr. 2008, pp. 349–366., doi: 10.1109/CPRE.2008.4515065.
- [2] W. Charytoniuk, W. J. Lee, M. S. Chen, J. Cultrera, and T. Maffetone, "Arcing fault detection in underground distribution networks feasibility study," in *IEEE Industrial and Commercial Power Systems Technical Conference. Conference Record*, 2000, pp. 15–20., doi: 10.1109/ICPS.2000.854352.
- [3] N. T. Stringer and L. A. Kojovic, "Prevention of underground cable splice failures," *IEEE Transactions on Industry Applications*, vol. 37, no. 1, pp. 230–239, 2001, doi: 10.1109/28.903154.
- [4] T. T. Newton and L. Kojovic, "Detection of sub-cycle, self-clearing faults." U.S. Patent No. 6,198,401, 1999.
- [5] E. C. Bascom, D. W. Von Dollen, and H. W. Ng, "Computerized underground cable fault location expertise," in *Proceedings of IEEE/PES Transmission and Distribution Conference*, 1994, pp. 376–382., doi: 10.1109/TDC.1994.328403.
- [6] A. D. Filomena, M. Resener, R. H. Salim, and A. S. Bretas, "Fault location for underground distribution feeders: an extended impedance-based formulation with capacitive current compensation," *International Journal of Electrical Power and Energy Systems*, vol. 31, no. 9, pp. 489–496, Oct. 2009, doi: 10.1016/j.ijepes.2009.03.026.
- [7] K. Zimmerman and D. Costello, "Impedance-based fault location experience," in *IEEE Rural Electric Power Conference*, 2006, pp. 1–16., doi: 10.1109/REPCON.2006.1649060.
- [8] E. O. Schweitzer, "A review of impedance-based fault locating experience," *14th Annual Iowa-Nebraska System Protection Seminar*, 1990
- [9] K. K. Kuan and K. Warwick, "Real-time expert system for fault location on voltage underground distribution cables," *IEE Proceedings C Generation, Transmission and Distribution*, vol. 139, no. 3, 235, 1992, doi: 10.1049/ip-c.1992.0036.
- [10] M. J. Mousavi, K. L. Butler-Purry, R. Gutierrez-Osuna, and M. Najafi, "Classification of load change transients and incipient abnormalities in underground cable using pattern analysis techniques," in *IEEE PES Transmission and Distribution Conference and Exposition*, 2003, vol. 1, pp. 175–180., doi: 10.1109/TDC.2003.1335177.
- [11] T. A. Kawady, A.-M. I. Taalab, and M. El-Sad, "An accurate fault locator for underground distribution networks using modified apparent-impedance calculation," in *10th IET International Conference on Developments in Power System Protection (DPSP 2010)*, 2010, vol. 2010, no. 558., doi: 10.1049/cp.2010.0302.
- [12] X. Yang, M.-S. Choi, S.-J. Lee, C.-W. Ten, and S.-I. Lim, "Fault location for underground power cable using distributed parameter approach," *IEEE Transactions on Power Systems*, vol. 23, no. 4, pp. 1809–1816, Nov. 2008, doi: 10.1109/TPWRS.2008.2002289.
- [13] M. M. Saha, "Fault location method for MV cable network," in *7th International Conference on Developments in Power Systems Protection (DPSP 2001)*, 2001, vol. 2001, pp. 323–326., doi: 10.1049/cp:20010165.
- [14] S. Jamali, "Fault location method for distribution networks using 37-buses distributed parameter line model," in *Eighth IEE International Conference on Developments in Power System Protection*, 2004, pp. 216–219., doi: 10.1049/cp:20040102.
- [15] T. Takagi, Y. Yamakoshi, M. Yamaura, R. Kondow, and T. Matsushima, "Development of a new type fault locator using the one-terminal voltage and current data," *IEEE Transactions on Power Apparatus and Systems*, no. 8, pp. 2892–2898, Aug. 1982, doi: 10.1109/TPAS.1982.317615.
- [16] M. Gilany, D. K. Ibrahim, and E. S. Tag Eldin, "Traveling-wave-based fault-location scheme for multiend-aged underground cable system," *IEEE Transactions on Power Delivery*, vol. 22, no. 1, pp. 82–89, Jan. 2007, doi: 10.1109/TPWRD.2006.881439.
- [17] V. Nazerian, A. T. Nasrabadi, and I. E. P. Afrakoti, "Switching characteristics of SOA-assisted all-optical sagnac interferometer switch for picosecond pulses," *Journal of Engineering and Applied Sciences*, vol. 11, no. 4, pp. 751–759, 2016, doi: 10.3923/jeasci.2016.751.759.
- [18] L. V. Bewley, "Traveling waves on transmission systems," *Transactions of the American Institute of Electrical Engineers*, vol. 50, no. 2, pp. 532–550, Jun. 1931, doi: 10.1109/T-AIEE.1931.5055827.
- [19] W. Zhao, Y. H. Song, and W. R. Chen, "Improved GPS travelling wave fault locator for power cables by using wavelet analysis," *International Journal of Electrical Power and Energy Systems*, vol. 23, no. 5, pp. 403–411, Jun. 2001, doi: 10.1016/S0142-0615(00)00064-8.
- [20] Z. Q. Bo, R. K. Aggarwal, A. T. Johns, and P. J. Moore, "Accurate fault location and protection scheme for power cable using fault generated high frequency voltage transients," in *Proceedings of 8th Mediterranean Electrotechnical Conference on Industrial Applications in Power Systems, Computer Science and Telecommunications (MELECON 96)*, 1996, vol. 2, pp. 777–780., doi: 10.1109/MELCON.1996.551330.
- [21] M. M. A. Aziz, E. S. Tag El Din, D. K. Ibrahim, and M. Gilany, "A phasor-based double ended fault location scheme for aged power cables," *Electric Power Components and Systems*, vol. 34, no. 4, pp. 417–432, 2006, doi: 10.1080/15325000500346743.
- [22] A. G. Phadke and J. S. Thorp, *Synchronized phasor measurements and their applications*. Boston, MA: Springer US, 2008, doi: 10.1007/978-0-387-76537-2.
- [23] M. Zadehbagheri, M. J. Kiani, T. Sutikno, and R. A. Moghadam, "Design of a new backstepping controller for control of microgrid sources inverter," *International Journal of Electrical and Computer Engineering (IJECE)*, vol. 12, no. 4,

- pp. 4469–4482, Aug. 2022, doi: 10.11591/ijece.v12i4.pp4469-4482.
- [24] Z. Chen, “Wavelet transform based accurate fault location and protection technique for cable circuits,” in *5th International Conference on Advances in Power System Control, Operation and Management*, 2000, vol. 2000, no. 478 I, pp. 59–63, doi: 10.1049/cp:20000364.
- [25] F. Provoost and W. Van Buijtenen, “Practical experience with fault location in MV cable networks,” in *IET Conference Publications*, 2009, no. 550., doi: 10.1049/cp.2009.0817.
- [26] P. M. Van Oirsouw and F. Provoost, “Fault localization in an MV distribution network,” in *17th International Conference on Electricity Distribution*, 2003, pp. 2–6.
- [27] J. Moshagh and R. Aggarwal, “A new approach to ungrounded fault location in a three-phase underground distribution system using combined neural networks & wavelet analysis,” in *Canadian Conference on Electrical and Computer Engineering*, 2006, pp. 376–381., doi: 10.1109/CCECE.2006.277594.
- [28] J. Sadeh and H. Afradi, “A new and accurate fault location algorithm for combined transmission lines using adaptive network-based fuzzy inference system,” *Electric Power Systems Research*, vol. 79, no. 11, pp. 1538–1545, Nov. 2009, doi: 10.1016/j.epr.2009.05.007.
- [29] E. Faraji, A. R. Abbasi, S. Nejatian, M. Zadehbagheri, and H. Parvin, “Probabilistic planning of the active and reactive power sources constrained to securable-reliable operation in reconfigurable smart distribution networks,” *Electric Power Systems Research*, vol. 199, Oct. 2021, doi: 10.1016/j.epr.2021.107457.
- [30] T. Aloui, F. Ben Amar, and H. H. Abdallah, “Modeling of a three-phase underground power cable using the distributed parameters approach,” in *Eighth International Multi-Conference on Systems, Signals and Devices*, Mar. 2011, pp. 1–6., doi: 10.1109/SSD.2011.5767405.
- [31] A. Edwards, H. Kang, and S. Subramanian, “Improved algorithm for detection of self-clearing transient cable faults,” in *IET 9th International Conference on Developments in Power Systems Protection (DPSP 2008)*, 2008, vol. 2008, no. 536, pp. 204–207, doi: 10.1049/cp:20080036.
- [32] Z. Nematzadeh, R. Ibrahim, A. Selamat, and V. Nazerian, “The synergistic combination of fuzzy C-means and ensemble filtering for class noise detection,” *Engineering Computations*, vol. 37, no. 7, pp. 2337–2355, Jun. 2020, doi: 10.1108/EC-05-2019-0242.
- [33] M. Zadehbagheri, R. Ildarabadi, and M. B. Nejad, “Review of the UPFC different models in recent years,” *International Journal of Power Electronics and Drive Systems (IJPEDS)*, vol. 4, no. 3, pp. 343–355, Sep. 2014, doi: 10.11591/ijpeds.v4i3.5982.
- [34] M. Popov, V. Terzija, Z. Radojevic, and G. Rietveld, “An efficient algorithm for fault location on mixed line-cable transmission corridors,” in *International Conference on Power Systems Transients*, 2013, no. 5, pp. 3–7.

BIOGRAPHIES OF AUTHORS



Vahdat Nazerian    received his B.Sc. degree from Iran University of Science and Technology, Tehran, Iran in 2003, M.Sc. and Ph.D. degrees from Khaje Nasir Toosi University of Technology, Tehran, Iran in 2005 and 2011, respectively, all in Electronics. He joined the Electrical Engineering Department of University of Mazandaran in 2014 as an assistant professor. His research and teaching concern semiconductor devices, analysis and fabrication. His research presently focuses on soft-computing, intelligent network, nanotechnology and application, renewable energy and optimization algorithms. He can be contacted at email: v.nazerian@umz.ac.ir.



Mohammad Esmaeil Zakerifar    received his B.Sc. degree from Iranica University, Mazandaran, Iran in 2011, M.Sc. degree from Islamic Azad University, Mazabdaran, Iran in 2017, both in Control Engineering. His current research interests include nanotechnology and application, power electronic, power systems, controller, and intelligence network. He can be contacted at email: mohammad.zakerifar@gmail.com.



Mahmoud Zadehbagheri    was born in Yasouj, Iran, in October 1979. He received a B.S. degree in Electrical Engineering from Kashan University, in 2003, an M.S. degree in Electrical Engineering from Islamic Azad University, Najafabad Branch, in 2008, and the joint Ph.D. degree in Electrical Engineering from Universiti Teknologi Malaysia (UTM), Johor, Skudai, Malaysia, and H.S University, Khorasan, Iran, in 2017. He is with the Department of the Electrical Engineering, Islamic Azad University, Yasouj Branch. His research interests include the fields of Power Electronics, Electrical Machines and Drives, FACTS devices, Renewable Energy, and Power Quality. He can be contacted at email: Ma.zadehbagheri@iau.ac.ir.



Mohammad Javad Kiani    was born in Yasouj, Iran. He received his B.S. and M.S. degrees in Electrical Engineering from the K. N. Toosi University of Technology, Tehran, Iran, in 2003 and 2008, respectively. He received his Ph.D. degree in Electrical Engineering from the Universiti Teknologi Malaysia (UTM), Johor, Skudai, Malaysia, in 2017. He is presently a faculty member in the Department of Electrical Engineering, Islamic Azad University, Yasouj, Iran. His current research interests include nanotechnology and application, power electronic, power systems, controller, and intelligence network. He can be contacted at email: MJ.kiani@iau.ac.ir.



Tole Sutikno    is a Lecturer in the Electrical Engineering Department at the Universitas Ahmad Dahlan (UAD), Yogyakarta, Indonesia. He received his B.Eng., M.Eng., and Ph.D. degrees in Electrical Engineering from Universitas Diponegoro, Universitas Gadjah Mada, and Universiti Teknologi Malaysia, in 1999, 2004, and 2016, respectively. He has been an Associate Professor at UAD, Yogyakarta, Indonesia since 2008. Since 2005, he has served as Editor-in-Chief of TELKOMNIKA, and since 2016, he has led the Embedded Systems and Power Electronics Research Group. His research interests include the fields of industrial applications, industrial electronics, industrial informatics, power electronics, motor drives, renewable energy, FPGA applications, embedded systems, image processing, artificial intelligence, intelligent control, digital design, and digital library. He can be contacted by email at tole@ee.uad.ac.id.